J Clust Sci (2017) 28:3021–3034
DOI 10.1007/s10876-017-1274-1

ORIGINAL PAPER

A New Organic–Inorganic Hybrid Compound $(C_7H_7N_2)_2[Cu_2Cl_6]$: Synthesis, Crystal Structure, Hirshfeld Surface Analysis, Vibrational and Thermal Properties

K. Azouzi[1] · B. Hamdi[1] · Abd. Ben Salah[1]

Received: 9 November 2016 / Published online: 24 August 2017

Abstract The present paper reports the chemical synthesis, structure study, Hirshfeld surface analyses, vibrational properties, and thermal analysis of new hybrid compound called: bis-benzymidazolium hexachlorodicuprate(II). It is crystallized in the monoclinic system $P2_1/n$ at room temperature with the following parameters: $a = 16.7794$ (18) Å, $b = 6.4216$ (6) Å, $c = 18.535$ (2) Å, $\beta = 92.931$ (8)°, and $Z = 8$. The structure of this compound might be described as layered with two parallel anionic and cationic layers. In this structure, the Cu^{2+} ion, surrounded by five chlorides, adopts the square pyramidal coordination geometry. The $[CuCl_5]^{2-}$ square pyramids sharing two common Cl atoms are held together forming chains of dimers of the form $[Cu_2Cl_6]^{2-}$. Network hydrogen-bonding and π–π interaction assures the cohesion between these layers and stabilizes the crystal. Hirshfeld surface analyses and fingerprint plots are used for decoding intermolecular interactions in the crystal network and contribution of component units for the construction of the 3D architecture. The vibration properties of this structure were studied by Raman scattering and infrared spectroscopies. Thermogravimetric analysis and differential scanning calorimetry measurements have been carried out on $(C_7H_7N_2)_2[Cu_2Cl_6]$ crystal in the temperature range between 275 and 500 K.

Keywords Crystal structure · Hirshfeld surface · Copper · FT-IR · Raman

Electronic supplementary material The online version of this article (doi:10.1007/s10876-017-1274-1) contains supplementary material, which is available to authorized users.

✉ K. Azouzi
azouzi.khaoula@yahoo.fr

[1] Laboratoire des Sciences des Matériaux et de l'Environnement, Faculté des Sciences de SFAX, University of SFAX, PB 1171, 3000 Sfax, Tunisia

Introduction

Copper was one of the earliest elements known to man. At one time, it could be found lying on the ground in its native state or uncombined state. Copper's distinctive red color made it easy to identify. Early humans used copper for many purposes. Copper's antimicrobial properties have made it a popular metal in the medical field. Multiple hospitals have experimented with covering frequently touched surfaces, such as bed rails and call buttons, with copper or copper alloys in an attempt to slow the spread of hospital-acquired infections [1]. Copper kills microbes by interfering with the electrical charge of the organisms' cell membranes. Copper also plays a huge role in electronics, and because of its abundance and low price tag, researchers are working to integrate the metal into an increasing number of cutting-edge devices. There are also many other uses for copper that have not been mentioned, such as for the production of art, jewelry, musical instruments, etching, engraving, and other things making the list of copper's applications somewhat endless.

Copper exhibits a variety of compounds, many of which are colored. The two principal oxidation states of copper are +1 and +2 although some +3 complexes are known. Copper(I) compounds are expected to be diamagnetic in nature and are usually colorless, except where color results from charge transfer or from the anion. The Cu^{+} ion has tetrahedral or square planar geometry. In solid compounds, copper(I) is often the more stable state at moderate temperatures.

The copper(II) ion is usually the more stable state in aqueous solutions. Compounds of this ion, often called cupric compounds, are usually colored. They are affected by Jahn–Teller distortions and exhibit a wide range of stereochemistry with four [2, 3], five [4, 5], and six coordination [6] compounds predominating. This article presents the synthesis of a Cu(II) complex with benzymidazole by slow evaporation method at room temperature.

So, the use of benzymidazole gives birth to a new $(C_7H_7N_2)_2[Cu_2Cl_6]$ complex, of which we managed to find single crystals. We are reporting the synthesis, X-ray crystal structure, Hirshfeld surface, vibrational studies, and thermal properties of the bis-benzymidazolium hexachlorodicuprate(II).

Experiment Section

Synthesis of $(C_7H_7N_2)_2[Cu_2Cl_6]$

Benzymidazole (purity 98) and copper(II) chloride dihydrate $(CuCl_2).2H_2O$ (purity 98%) were dissolved in a (1 M) HCl aqueous solution in a molar ratio of 2:1 and stirred for a few minutes. Suitable crystals for X-ray structure determination were obtained by slow evaporation at room temperature over several days. The reactions sequence for the synthesis is shown in the following equation:

$$2(C_7H_6N_2)^+ + 2(CuCl_2 \cdot 2H_2O) \xrightarrow{HCl} (C_7H_7N_2)_2Cu_2Cl_6 + H_2O$$

Density was measured at room temperature by flotation in toluene. The density average value D_m (mg m^{-3}) = 1.63 (6) was found to be in good agreement with the calculated one D_x (mg m^{-3}) = 1.925.

Characterization

A single crystal was selected in order to perform its structural analysis by an X-ray diffraction. The crystallographic data was carried out on an Apex II Kappa CCD area detector diffractometer using the KαMo radiation (λ = 0.71073 Å).

The positional parameters of heavy atom of copper and chlorine were determined by the Patterson method with the SHELXS-97 program [7] in the space group $P2_1/n$. The nitrogen and carbon atoms were determined from successive difference Fourier map with anisotropic temperature factor using SHELXL-97 program [8]. The pertinent experimental details of the structure determination for the new compounds are presented in Table 1. All the hydrogen atoms were placed geometrically and refined isotropically. The last cycle of refinement included the atomic coordinates for all the atoms, anisotropic thermal parameters and isotropic thermal whose values are listed in table S.1 and table S.2.

The structure input file in cif format was used to calculate the Hirshfeld surfaces and the associated 2D-fingerprint plots using Crystal Explorer [9]. The Hirshfeld surface enclosing a molecule is defined by points where the contribution to the electron density from the molecule of interest is equal to the contribution from all the other molecules. For each point on that isosurface two distances are defined: d_e, the distance from the point to the nearest nucleus external to the surface, and d_i the distance to the nearest nucleus internal to the surface. The normalized contact distance (d_{norm}) based on d_e and d_i was given by:

$$d_{norm} = \frac{d_i - r_i^{vd\omega}}{r_i^{vd\omega}} + \frac{d_e - r_e^{vd\omega}}{r_e^{vd\omega}}$$

where, $r_i^{vd\omega}$ and $r_e^{vd\omega}$ are the van der Waals radii of the appropriate atoms internal and external to the surface, respectively [10, 11].

The IR spectrum was recorded in the range 4000–400 cm^{-1} with a "Nicolet Impact 410" spectrometer using a simple dispersed pure KBr pressed into pellet. Raman scattering was performed at room temperature using a LABRAM-Jobin–Yvon set up. The excitation line was the 630 nm from a Neon laser in the range 50–1000 cm^{-1}. The incident laser power was limited to 5 mW to avoid sample heating degradation.

The thermal behavior was studied under an air flow in Mettler Toledo DSC 822^e calorimeter and Perkin Elmer Pyris 6 TGA equipment in the 275–500 K temperature range with a scanning rate of 5 °C/min.

Table 1 Summary of crystal data, intensity measurements, and refined parameters of the $(C_7H_7N_2)_2[Cu_2Cl_6]$ compound

Crystal data	
Empirical formula	$(C_7H_7N_2)_2[Cu_2Cl_6]$
Crystal system	Monoclinic
Space group	$P2_1/n$
a (Å)	16.7794 (18)
b (Å)	6.4216 (6)
c (Å)	18.535 (2)
β (°)	92.931 (8)
Volume (Å^3)	1994.5 (4)
Z	8
D_{calc} (mg m^{-3})	1.925
Crystal size (mm^3)	0.43 × 0.32 × 0.22
F(000)	1144
Crystal color	Vert
Data collection	
Temperature (K)	293
λ (MoKα) (Å)	0.71073
Reflections collected	27,893
Independent reflections	4111
Reflections with $I > 2\sigma(I)$	2288
Limiting indices	h = −20 → 21.k = −7 → 7.l = −23 → 23
Refinement	
Refinement method	Full-matrix least-squares on F^2
$R[F^2 > 2\sigma(F^2)]$	0.04
$wR(F^2)$	0.12

Results and Discussion

Structure Description

Structural determination at room temperature shows that the title compound crystallizes in the monoclinic system, space group $P2_1/n$, with the lattice constants of a (Å) = 16.7794 (18), b (Å) = 6.4216 (6), c (Å) = 18.535 (2), β (°) = 92.931 (8). The unit cell volume is 1994.5 (4) Å^3 with $Z = 8$ formula units. A view of the asymmetric unit of the structure drawn with 50% probability thermal ellipsoids is shown in Fig. 1 and consists of two benzymidazolium cations and two $[CuCl_3]^-$ anions. The anions generate an inversion center in order to form a Cu_2Cl_6 dimer constituted of two square pyramids $[CuCl_5]^{3-}$ which are sharing one edge.

The projection along the c axis of the atomic arrangement is illustrated in Fig. 2. As it can be observed from this figure, the atomic arrangement can be described by an alternation of organic and inorganic layers along the b axis. Each organic layer is

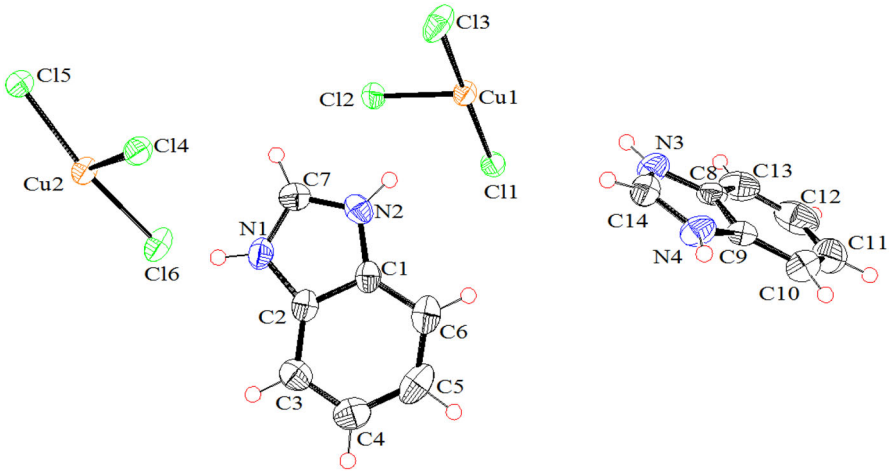

Fig. 1 A view of the asymmetric unit of $(C_7H_7N_2)_2[Cu_2Cl_6]$

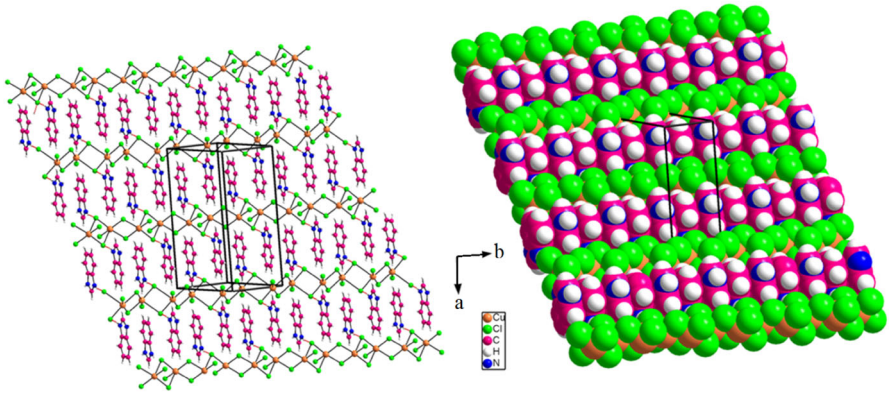

Fig. 2 Packing diagram showing the alternation between different entities in $(C_7H_7N_2)_2[Cu_2Cl_6]$

formed by $(C_7H_7N_2)^+$ cations, whereas the inorganic layer is built up by infinite chains of $[Cu_2Cl_6]^{2-}$ anions parallel to the [010] direction. The two negative charges of the anionic species are contra balanced by the two positive charges of the organic cation.

The inorganic anion consists of two crystallographically independent Cu atoms: Cu_1 and Cu_2. The description of a $[Cu_2Cl_6]^{2-}$ entity is justified by quasi-equivalent Cu_1-Cl and Cu_2-Cl bonds distances.

The Cu–Cl bond lengths fall in the range 2.2490 (16) Å–2.8098 (16) Å and the Cl–Cu–Cl bond angles vary from 90.80 (7)° to 173.72 (6)°. The $[Cu_2Cl_6]^{2-}$ entities are located at $x = 0$, $y = ½$ (Fig. 3). The geometrical features of $(CuCl_5)^{3-}$ entities are reported on Table 2.

The organic part of bis-benzymidazolium hexachlorodicuprate(II) compound is formed by two types of cation: $(C_7H_7N_2)^+$ (I) and $(C_7H_7N_2)^+$ (II), each cation is

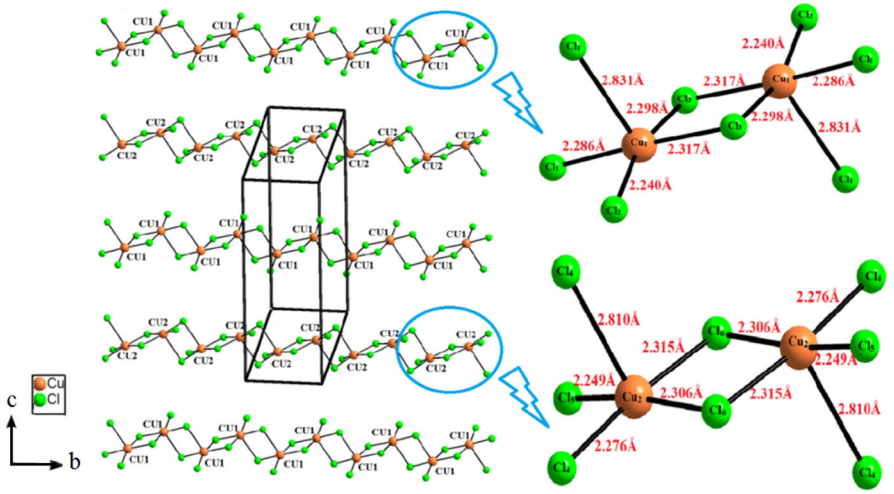

Fig. 3 Projection along the a axis of the inorganic arrangement of $(C_7H_7N_2)_2[Cu_2Cl_6]$

Table 2 Selected bond length (Å) and bond angles (°) for inorganic anion

Bond length (Å)		Bond angles (°)	
$[Cu_1Cl_5]$			
Cu1–Cl3	2.298 (8)	Cl1–Cu1–Cl3	102.66 (6)
Cu1–Cl2	2.2397 (17)	Cl1–Cu1–Cl3	172.62 (7)
Cu1–Cl3	2.317 (2)	Cl1–Cu1–Cl3	91.68 (6)
Cu1–Cl1	2.2856 (16)	Cl2–Cu1–Cl3	90.80 (7)
Cu1–Cl1	2.8313 (16)	Cl1–Cu1–Cl2	92.92 (6)
		Cl2–Cu1–Cl3	163.83 (8)
		Cl1–Cu1–Cl2	93.21 (6)
		Cl1–Cu1–Cl3	98.16 (6)
$[Cu_2Cl_5]$			
Cu2–Cl4	2.2758 (16)	Cl4–Cu2–Cl5	92.1 (6)
Cu2–Cl5	2.2490 (16)	Cl4–Cu2–Cl6	91.73 (6)
Cu2–Cl6	2.3060 (16)	Cl5–Cu2–Cl6	91.70 (6)
Cu2–Cl6	2.3144 (16)	Cl5–Cu2–Cl6	167.84 (7)
Cu2–Cl4	2.8098 (16)	Cl4–Cu2–Cl6	173.72 (6)
		Cl4–Cu2–Cl6	99.90 (5)
		Cl4–Cu2–Cl5	91.79 (6)
		Cl4–Cu2–Cl6	99.33 (5)

created by two rings. In the first cation $(C_7H_7N_2)^+$ (I), the interatomic distances C–C and N–C are in the ranges of 1.362 (9)–1.404 (10) Å and 1.308 (8)–1.381 (8) Å, respectively. The C–C–C and C–N–C angle values vary from 115.0 (6) to 122.5 (6)° and from 106.3 (6) to 132.2 (5)°, respectively. While in the second cation $(C_7H_7N_2)^+$ (II), the C–C bond lengths vary from 1.366 (11) to 1.396 (9) Å. The N–C

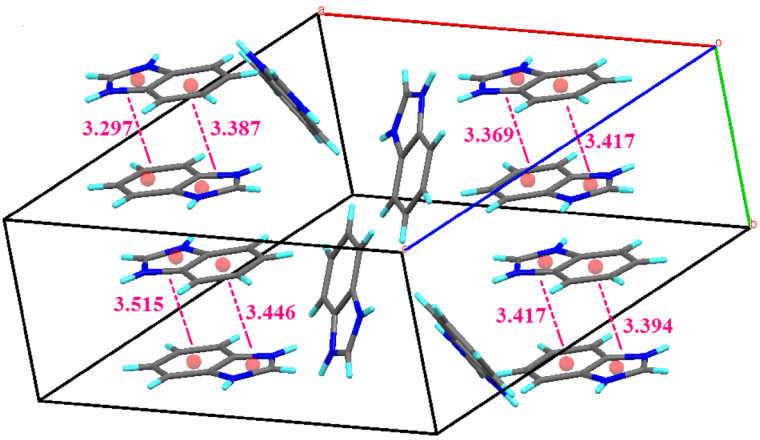

Fig. 4 The alternating rows of π–π interacting rings in the different altering of the organic molecule

bond lengths vary from 1.309 (8) to 1.392 (8) Å. The C–C–C and C–N–C angles vary from 105.5 (5) to 131.6 (6)° and 116.8 (6) to 123.1 (7)°, respectively.

The organic group is located in the (a b) plane at approximately $y = 1/4$ and $y = 3/4$. Main geometrical characteristics of these cations are summarized in table S.3.

The rings of successive cations are approximately parallel to each other and are equidistant: adjacent rings are separated by centroid-to-centroid distances varying from 3.297 to 3.515 Å, which are considered a π–π stacking interactions [12, 13]. The geometry of the π–π stacks is presented in Fig. 4.

Figure 5 shows a perspective view of the crystal structure, together with the network of hydrogen contacts (dotted lines). The intermolecular hydrogen bonding contacts N–H···Cl, and C-H···Cl provide a linkage between the $(C_7H_7N_2)^{2+}$ entities and the $[Cu_2Cl_6]^{2-}$ anions (table S.4). Each cation forms two or three hydrogen bonds with different anions, forming a three dimensional network such that all the hydrogen atoms bonded to nitrogen atoms participate in the formation of these hydrogen bonds.

Hirshfeld Surface

The Hirshfeld surfaces of $(C_7H_7N_2)_2[Cu_2Cl_6]$ complex is displayed in Fig. 6a, showing surface that have been mapped over a d_{norm}. The Hirshfeld surface surrounded the asymmetric unit is constructed basing on the electron distribution calculated as the sum of spherical atom electron densities.

For each point on that isosurface two distances are determined: one is d_e represents the distance from the point to the nearest nucleus external to the surface and second one is d_i represents the distance to the nearest nucleus internal to the surface. The normalized contact distance (d_{norm}) based on both d_e and d_i. The surfaces are shown as transparent to allow visualization of the asymmetric unit molecule, around which they were calculated. The surface represents the circular

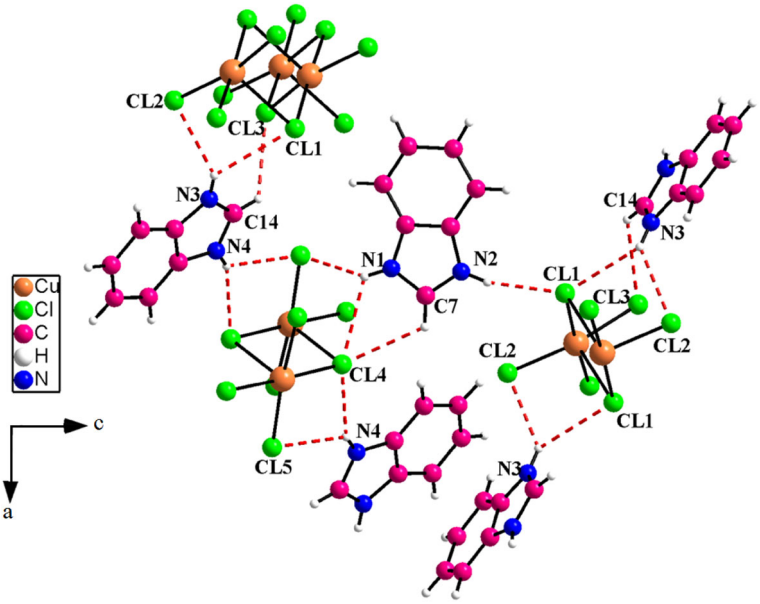

Fig. 5 The drawing show the intermolecular hydrogen bonds contacts which are represented by *dotted line* for $(C_7H_7N_2)_2[Cu_2Cl_6]$ crystal

depressions (deep red) visible on the Hirshfeld surface indicative of hydrogen bonding contacts [14, 15].

The fingerprint plots can be decomposed to highlight particular atom pair close contacts and this decomposition enables separation of contributions from different interaction types, which overlap in the full fingerprint. The 2D fingerprint plots are displayed by using the expanded 0.6–2.8 Å view with the d_e and d_i distance scales on the graph axes (Fig. 6b).

The close Cl···H/H···Cl intercontacts cover about 46% of the Hirshfeld surface areas, represented at the plot as two distinct spikes of almost equal lengths (Cl···H corresponds to a spike in the bottom left area, donor, while H···Cl e in the bottom right region, acceptor).

The H···H interactions, which were reflected in the middle of scattered points in the 2D fingerprint plots, have the second most significant contribution to the total Hirshfeld surfaces, which comprise 17.8%.

The points in the (d_i, d_e) and (d_e, d_i) regions of (1.25 Å, 1.05 Å) and (1.05 Å, 1.25 Å) in the finger print plot is due to Cu–Cl and Cl–Cu interactions, respectively. The proportions of Cu···Cl/Cl···Cu interactions comprising 11.4% of the total Hirshfeld surface of the molecule.

The C···H/H···C intermolecular interactions appear as distinct spikes in the 2D fingerprint plot (Fig. 6c). Complementary regions are visible in the fingerprint plots where one molecule act as donor ($d_e > d_i$) and the other as an acceptor ($d_e < d_i$).

Figure 7 contains the percentages of contributions for a variety of contacts in the title crystal structure.

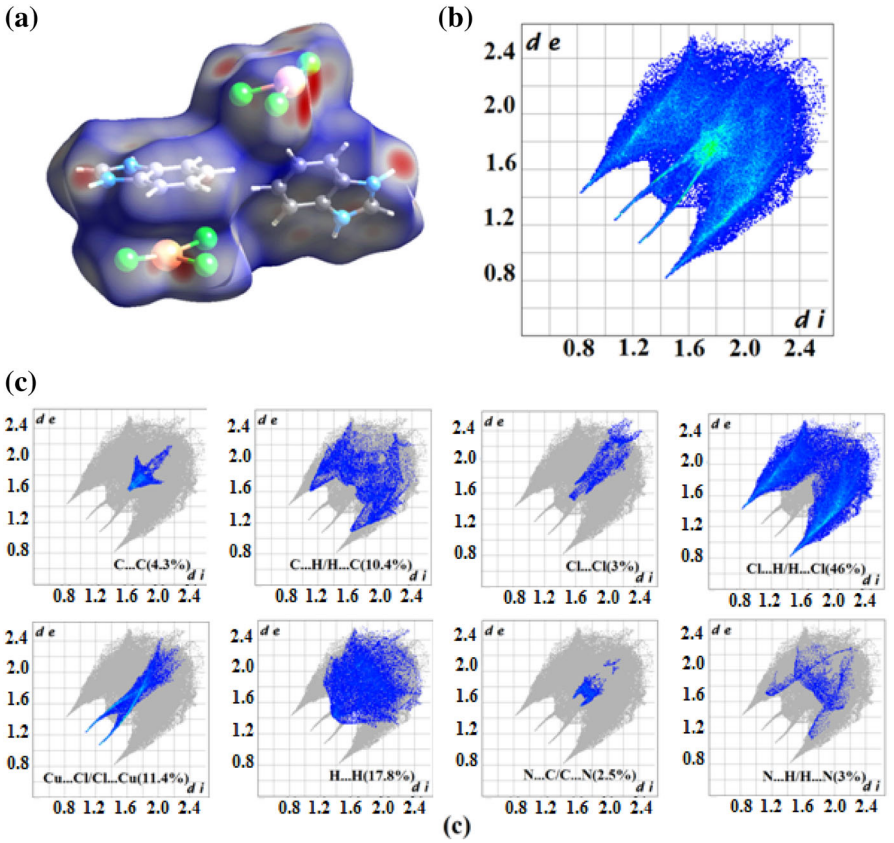

Fig. 6 **a** The Hirshfeld surface for bis-benzymidazolium hexachlorodicuprate(II) mapped with d_{norm} function; **b** the corresponding 2D fingerprint plot; **c** the fingerprint plots broken down into contributions from different contacts

The Shape index is the measurement of "which shape'', the red triangles on Shape index represent concave regions indicating atoms of the π–π stacked molecule above them, and the blue triangles represent convex regions indicating the ring atoms of the molecule inside these surfaces. Figure 8 showed the presence of red triangles on Shape index indicating π–π stacking of the molecules [16].

The Curvedness conveys the similar information as Shape index, which is the measurement of ''how much shape''. The large flat region delineated by a blue outline on the Curvedness surfaces indicating π–π stacking of the molecules. Figure 8, clearly shown that the area of the flat regions delineated by a blue outline [17].

Vibrational Studies

To gain more information on the crystal structure, we have undertaken a vibrational study using Raman scattering and infrared spectroscopy at room temperature. The

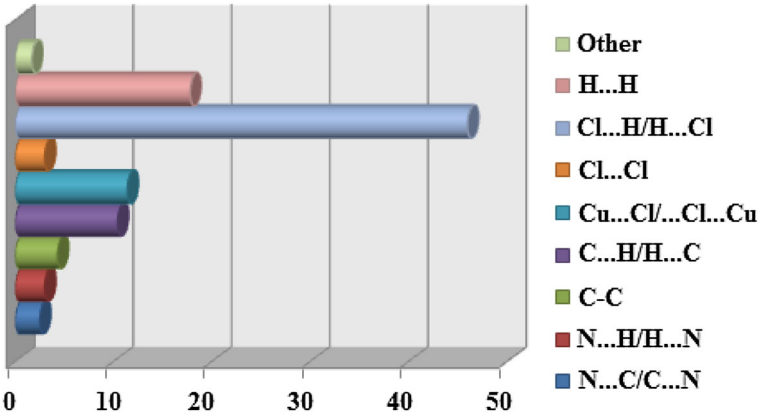

Fig. 7 Relative contributions to the % of Hirshfeld surface area for the various intermolecular contacts in $(C_7H_7N_2)_2[Cu_2Cl_6]$

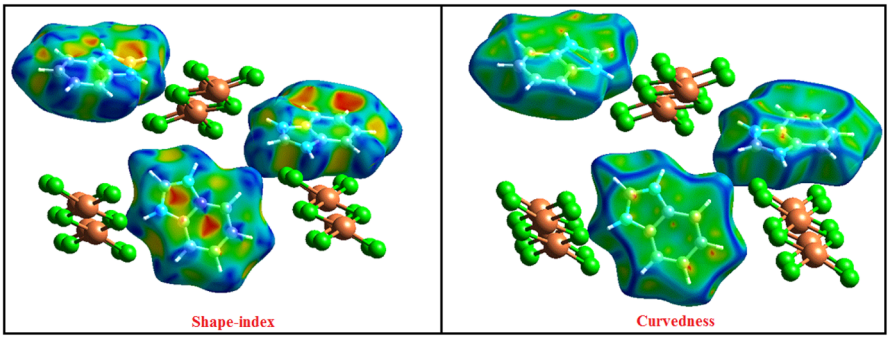

Fig. 8 The Hirshfeld surface of the title complex mapped with shape index and curvedness

Raman and the infrared spectra of the $(C_7H_7N_2)_2[Cu_2Cl_6]$ are showing in Figs. 9 and S.1 respectively. Using previous works reported in the literature on similar compounds [18, 19]; we propose in Table 3 an attempt of assignment of the main bands.

Anionic Vibrational Analysis

The bands corresponding to the internal vibrational modes of the $(CuCl_5)^{3-}$ anion appear in the Raman spectral below 400 cm^{-1}. The assignment of these bands was essentially made by comparison with compounds containing $(CuCl_5)^{3-}$ [20, 21]. The vibrational modes of $(CuCl_5)^{3-}$ give rise to two bands: one band observed at 244 cm^{-1} assigned to the Cu–Cl asymmetric stretching, the other is located at 226 cm^{-1} corresponding to ν_s (Cu–Cl). The weak bands observed at 120 and 75 cm^{-1} correspond to the Cl–Cu–Cl asymmetric and symmetric deformations modes.

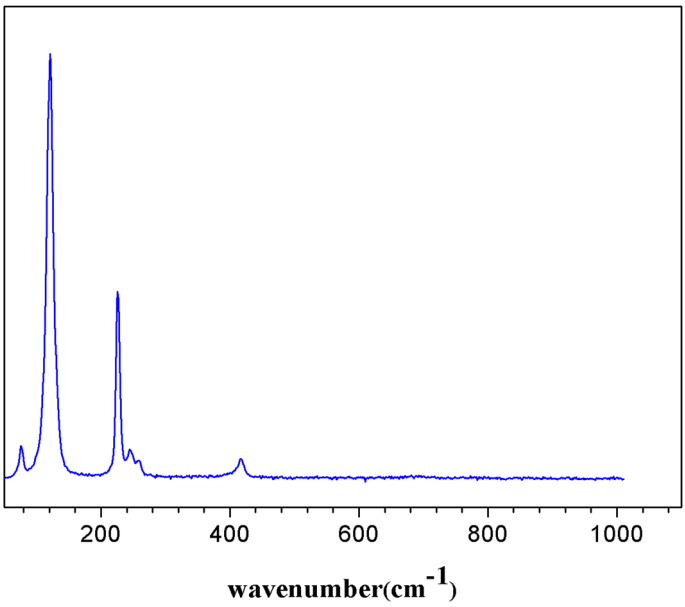

Fig. 9 Raman spectrum of $(C_7H_7N_2)_2[Cu_2Cl_6]$ at room temperature

Table 3 Observed vibration frequencies (cm^{-1}) of $(C_7H_7N_2)_2[Cu_2Cl_6]$ and proposed assignements

IR wavenumbers (cm^{-1})	Raman wavenumbers (cm^{-1})	Assignment
3450		(N–H) asymmetric stretching
3245		(N–H) symmetric stretching
1630		υ (C–C) β(N–H) υ(C=N)
1485		(N–H) bending
1440		(C=C) symmetric stretching
1365		(C=C) asymmetric stretching
1260		(C–H) in plane bending
1135		(C–H) out of plane bending
1005		(C–N) asymmetric stretching
755		(N–H) wagging
595		(C–N–C) scissoring
	244	(Cu–Cl) asymmetric stretching
	226	(Cu–Cl) symmetric stretching
	120	δas(Cl–Cu–Cl)
	75	δs((Cl–Cu–Cl))

Cationic Vibrational Analysis

We now discuss the internal modes of the organic cation observed in the IR spectra between 400 and 4000 cm^{-1} frequency range. The benzymidazolium group contains 16 atoms. For this number of atoms, $3 * 16 - 6 = 42$ internal modes are present. The high frequencies domain in the spectrum is generally characterized by (N–H) stretching modes. In the present study, the symmetric and asymmetric stretching vibrations of (N–H) are observed at 3245 and at 3450 cm^{-1}, respectively.

Besides, the two weak bands observed at 1440 and 1365 cm^{-1} were assigned to symmetric and asymmetric stretching vibrations of the (C=C). The in plane bending of the C–H is observed at 1260 cm^{-1} in the IR spectrum, while the out of plane bending appears at 1135 cm^{-1}. Concerning the wavenumbers found between 925 and 595 cm^{-1}, they are attributed to (C–C–N) and (C–C–C) deformation.

Thermal Study

DSC and TGA Analyses

The thermal behavior of the crystal was studied by employing thermogravimetric (TG) and differential scanning calorimetry (DSC). The DSC curves obtained for the $(C_7H_7N_2)_2[Cu_2Cl_6]$ crystals at a heating rate of 5 °C/mn with a temperature range of 275–500 K are illustrated in Fig. 11. The thermogram shows four endothermic peaks at 371, 414, 448 and 481 K.

The first peak located at 371 K corresponds to evaporation of water molecules, whilst the peak observed at 414 K corresponds to a single phase transition. The third peak was observed at 448 K, which corresponded to the fusion of the compound. The last peak observed at 481 K corresponding to the decomposition of $(C_7H_7N_2)_2[Cu_2Cl_6]$.

Additionally, the TGA curves were performed with a heating rate of 5 °C/min between 275 and 500 K as shown in Fig. 10 and shows that the compound exhibits two weight losses. The first one is of 14% from 360 to 379 K showed the loss of the water surface. The second one is from 470 K corresponding to the decomposition of $(C_7H_7N_2)_2[Cu_2Cl_6]$.

To demonstrate the reversibility of the observed transition, a differential-scanning calorimetry (DSC) measurement of sample for the title compound was carried out from 280 to 420 K at 5 °C/mn. Figure S.2 shows the appearance of only one reversible phase transition of first-order at $T = 414$ K in the heating cycle and at $T = 398$ K in the cooling cycle.

FT-IR Spectra

The IR spectra for the $(C_7H_7N_2)_2[Cu_2Cl_6]$ compound measured between 323 and 443 K for the wavenumber region [400 cm^{-1}–4000 cm^{-1}] are shown in Fig. 11. This analysis was performed to gain insights on the further top crystal dynamics and the mechanisms involved in the transition. For clarity zooming has been performed on the [3800–2600 cm^{-1}]. Marked changes were observed only in the high-frequency region. The positions of most of the analyzed bands are constant. The

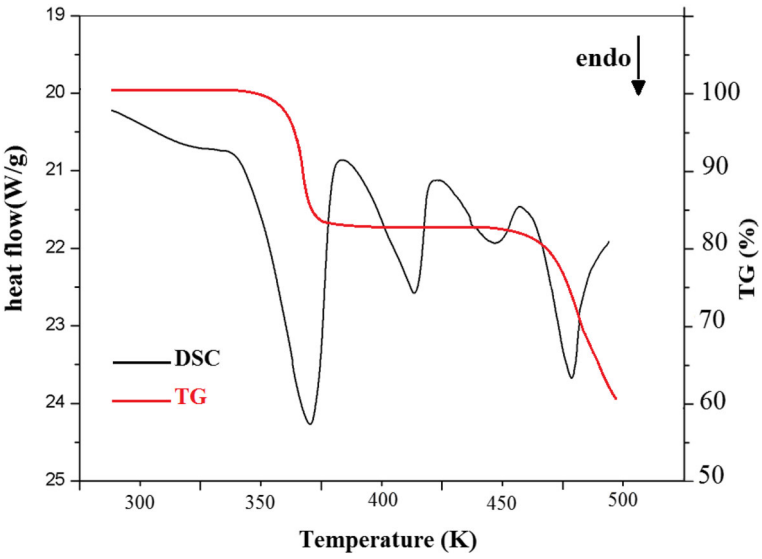

Fig. 10 TGA and DSC curves of $(C_7H_7N_2)_2[Cu_2Cl_6]$ crystal

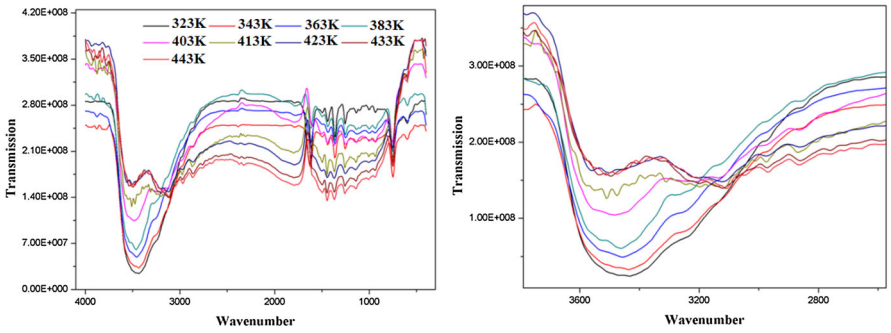

Fig. 11 Temperature dependences of IR spectra of $(C_7H_7N_2)_2[Cu_2Cl_6]$

difference is seen for the symmetric and asymmetric stretching vibrations of (N–H) observed between 3500 and 3050 cm^{-1}, which is probably due to the N–H···Cl hydrogen bond. However, the marked changes were observed as from the temperature 413 K. We can conclude that the transformation observed at T = 414 K in the DSC related with a phase transformation caused by a slight deformation of the organic group.

Conclusion

This paper report the syntheses, the studies by X-ray structure, vibrational properties (IR and Raman), and thermal measurement of a new compound bis-benzymidazolium hexachlorodicuprate(II). The atomic arrangement of this compound can be

described by the alternation of organic- inorganic layers. The material cohesion of the compound is assured by hydrogen bonds (N–H···Cl and C-H···Cl) established between anions and cations and π–π stacking interactions established between parallels cations. Infrared and Raman spectroscopy confirms the presence of organic cation $(C_7H_7N_2)^{2+}$and inorganic anion $[Cu_2Cl_6]^{2-}$. The measurements of DSC and ATG combined with IR indicate the existence of a phase transformation caused by a slight deformation of the organic group.

Supplementary Material

Crystallographic data for the title compound, have been deposited at the Cambridge Crystallographic Data Centre as supplementary publication CCDC 1515059 copies of these data can be obtained, free of charge, on application to CCDC, 12 Union Road, Cambridge CB21EZ, UK (fax: +44(0)-1223-336033 or Email: deposit@ccdc.cam.ac.uk).

References

1. R. Elayaperumal and P. Dharmalingam (2013). *Der Chem. Sin.* **2**, 170.
2. C. Peng (2011). *Acta Cryst.* **67**, 979.
3. S. Bouacida, R. Bouchene, A. Khadri, R. Belhouas, and H. Merazig (2013). *Acta Crystallogr. Sect. E* **69**, 610.
4. A. Kessentini, M. Belhouchet, J. J. Suñol, Y. Abid, and T. Mhiri (2015). *Spectrochim. Acta A Mol. Biomol. Spectrosc.* **134**, 28.
5. P. Arularasan, B. Sivakumar, G. Chakkaravarthi, and R. Mohana (2013). *Acta Cryst. E* **69**, 583.
6. T. Dammak, H. Boughzala, A. Mlayah, and Y. Abid (2016). *J. Lumin.* **173**, 213.
7. G.M. Sheldrick, SHELXS-86, *Program for Crystal Structure Solution* (University of Göttingen, Germany, 1986).
8. G.M. Sheldrick, SHELXL-97, *Program for Crystal Structure Refinement* (University of Göttingen, Germany, 1997).
9. S. K. Wolff, D. J. Grimwood, J. J. McKinnon, M. J. Turner, D. Jayatilaka, and M. A. Spackman, *Crystal Explorer ver. 3.1* (University of Western Australia, Perth, 2013).
10. A. M. Spackman and J. J. McKinnon (2002). *Cryst. Eng. Comm.* **66**, 378.
11. J. J. McKinnon, D. Jayatilaka, and M. A. Spackman (2007). *Chem. Commun.* **220**, 3814.
12. N. Karaa, B. Hamdi, A. Ben Salah, and R. Zouari (2012). *J. Mol. Struct.* **1013**, 168.
13. S. Chaouachi, S. Elleuch, B. Hamdi, and R. Zouari (2016). *J. Mol. Struct.* **1125**, 149.
14. S. Saha, A. Sasmal, C. R. Choudhury, G. Pilet, and A. Bauzá (2015). *Inorg. Chim. Acta* **425**, 211.
15. A. Frontera, S. Chakraborty, and S. Mitra (2015). *Inorg. Chim. Acta* **425**, 211.
16. Y. H. Luo, L. J. Yang, G. Han, Q. L. Liu, W. W. Ling, and B. W. Sun (2014). *J. Mol. Struct.* **1076**, 679.
17. H. Khanam, A. Mashrai, N. Siddiqui, M. Ahmad, M. J. Alam, and S. Ahmad (2015). *J. Mol. Struct.* **1084**, 274.
18. N. A. Abood, M. AL-Askari, A. Bahjat, and S. Basrah (2012). *J. Sci.* **30**, 119.
19. A. Suwaiyan, R. Zwarich, and N. Baig (1990). *J. Raman Spectrosc.* **21**, 243.
20. A. Kessentini, M. Belhouchet, J. J. Suñol, Y. Abid, and T. Mhiri (2015). *Spectrochim. Acta A* **134**, 28.
21. A. Kessentini, M. Belhouchet, Y. Abid, C. Minot, and T. Mhiri (2014). *Spectrochim. Acta A* **122**, 476.